

Rubidium-82 PET-CT for quantitative assessment of myocardial blood flow: validation in a canine model of coronary artery stenosis

Riikka Lautamäki · Richard T. George ·
Kakuya Kitagawa · Takahiro Higuchi ·
Jennifer Merrill · Corina Voicu · Anthony DiPaula ·
Stephan G. Nekolla · João A. C. Lima ·
Albert C. Lardo · Frank M. Bengel

Received: 31 July 2008 / Accepted: 15 September 2008 / Published online: 5 November 2008
© Springer-Verlag 2008

Abstract

Purpose Absolute quantification of myocardial blood flow expands the diagnostic potential of PET for assessment of coronary artery disease. ^{82}Rb has significantly contributed to increasing utilization of PET; however, clinical studies are still mostly analysed qualitatively. The aim of this study was to reevaluate the feasibility of ^{82}Rb for flow quantification, using hybrid PET-CT in an animal model of coronary stenosis.

Methods Nine dogs were prepared with experimental coronary artery stenosis. Dynamic PET was performed for

8 min after ^{82}Rb (1480–1850 MBq) injection during adenosine-induced vasodilation. Microspheres were injected simultaneously for reference flow measurements. CT angiography was used to determine the myocardial regions related to the stenotic vessel. Two methods for flow calculation were employed: a two-compartment model including a spill-over term, and a simplified retention index.

Results The two-compartment model data were in good agreement with microsphere flow ($y=0.84x + 0.20$; $r=0.92$, $p<0.0001$), although there was variability in the physiological flow range <3 ml/g per minute ($y=0.54x + 0.53$; $r=0.53$, $p=0.042$). Results from the retention index also correlated well with microsphere flow ($y=0.47x + 0.52$; $r=0.75$, $p=0.0004$). Error increased with higher flow, but the correlation was good in the physiological range ($y=0.62x + 0.29$; $r=0.84$, $p=0.0001$).

Conclusion Using current state-of-the-art PET-CT systems, quantification of myocardial blood flow is feasible with ^{82}Rb . A simplified approach based on tracer retention is practicable in the physiological flow range. These results encourage further testing of the robustness and usefulness in the clinical context of cardiac hybrid imaging.

Keywords Cardiology PET · PET-CT hybrid imaging · Myocardial blood flow · Rubidium-82

Drs. Lautamäki and George contributed equally to this study.

R. Lautamäki · T. Higuchi · J. Merrill · C. Voicu ·
F. M. Bengel (✉)

Department of Radiology, Division of Nuclear Medicine,
Johns Hopkins Medical Institutions,
601 N Caroline St,
Baltimore, MD 21210, USA
e-mail: fbengel1@jhmi.edu

R. T. George · K. Kitagawa · A. DiPaula · J. A. C. Lima ·
A. C. Lardo

Department of Medicine, Division of Cardiology,
Johns Hopkins Medical Institutions,
Baltimore, MD, USA

A. C. Lardo
Department of Biomedical Engineering,
Johns Hopkins Medical Institutions,
Baltimore, MD, USA

S. G. Nekolla
Nuklearmedizinische Klinik und Poliklinik,
Klinikum rechts der Isar, Technischen Universität München,
Munich, Germany

Introduction

The success of positron emission tomography (PET) in oncology, and the advent of hybrid PET-CT have resulted

in an increasing availability and utilization of PET for the clinical assessment of myocardial perfusion [1–6]. ^{82}Rb plays a key role in the clinical success of myocardial perfusion PET because it is a very short-lived generator product, it is readily available at sites without a cyclotron, and it enables high throughput for clinical rest–stress studies. While the tracer was initially used successfully mostly in North America, it has recently also been used clinically in Europe [7, 8].

Although ^{82}Rb was introduced decades ago [9–13], its current clinical use is still limited to qualitative analysis of regional relative tracer distribution. Absolute quantification of myocardial blood flow (MBF) may help identify patients with balanced ischaemia as an expression of extensive multivessel coronary disease [14] and it may help identify those with global microvascular/endothelial dysfunction as a precursor of clinically overt coronary disease [15–17]. Several studies have proposed algorithms to quantify MBF from dynamic ^{82}Rb datasets [9, 10, 12, 18–21]. However, laborious handling and processing of dynamic data, the tracer characteristics of ^{82}Rb (which result in estimation errors for MBF due to nonlinear extraction at higher flow), and the physical characteristics of ^{82}Rb (consisting of a high positron energy which degrades image quality, and an ultrashort half-life which makes it difficult to balance high count rates and scanner dead-time problems at the beginning of the acquisition and low count rates and image noise in later phases) are complications that have hindered clinical acceptance.

The newest generation of PET systems now provide detector materials with better count rate performance and shorter dead time [22]. Software for efficient acquisition and handling of list-mode data is available, which allows post-hoc generation of dynamic sequences without affecting routinely used gated and static images. And finally, PET scanners are integrated with multislice CT for hybrid imaging of cardiac morphology and function, resulting in additional technical challenges [23], but also significant opportunities [24]. Using a scanner system which includes all of the above advances, we revisited the feasibility of MBF quantification with ^{82}Rb in the present study by using previously introduced algorithms in an animal model of coronary stenosis.

Materials and methods

Animal model

The Animal Care and Use Committee of Johns Hopkins University approved all procedures. Nine mongrel dogs (22–32 kg) were anaesthetized with intravenous thiopental (3–4 mg/kg), intubated, and mechanically ventilated with isoflurane anaesthesia (1–2%). Following vascular cut

downs, 8F sheaths were placed in the femoral veins, right femoral artery, and right internal jugular vein. Left thoracotomy was performed and the pericardium was excised. A catheter was placed in the left atrium and the proximal descending aorta for radioactive microsphere administration and sampling. The proximal-to-mid left anterior descending artery ($n=4$) or the proximal left circumflex artery ($n=5$) was instrumented with an electromagnetic flow probe and reactive hyperaemia was tested with an inflatable external occluder. A suture was then secured around the vessel and tightened to produce a graded stenosis aimed to maintain baseline flow, but attain a 50% or more reduction in hyperaemic flow. The thoracotomy was closed and the animal was transported to the PET-CT scanner using a portable ventilator.

PET-CT protocol

PET-CT imaging was performed using a GE Discovery Rx VCT scanner (GE Medical Systems, Milwaukee, WI), equipped with a LYSO PET component and a 64-slice CT component. Compared to conventional PET scanners with BGO crystals, this new scanner has a shorter dead time and fewer random events, increasing the sensitivity especially during high count rate conditions [22].

The dogs were positioned supine in a cradle and a CT scout scan, followed by a low-dose CT scan (120 kV, 80 mA) for attenuation correction were obtained. Intravenous adenosine infusion was started, and ^{82}Rb was infused intravenously after 2 min into the adenosine (60–90 s slow bolus, 1480–1850 MBq). For six dogs, the adenosine dose was the clinical standard of 140 $\mu\text{g}/\text{kg}$ per minute but since the maximal hyperaemic conditions, i.e. high values of MBF in the remote myocardium, were difficult to achieve in these animals, we used a higher dose of 420 $\mu\text{g}/\text{kg}$ per minute in three dogs. List-mode PET data acquisition (VIP, GE Healthcare, Waukesha, WI) was started with tracer infusion and was continued for 8 min. Approximately two million radioactive microspheres (^{57}Co , ^{46}Sc , ^{95}Nb , ^{141}Ce or ^{85}Sr ; Perkin-Elmer) were injected 1 min after ^{82}Rb into the left atrium with simultaneous collection of reference blood samples from the descending aorta at a rate of 2.16 ml/min for 5 min.

After the PET scan, coronary CT angiography (CTA) was performed. Immediately prior to acquisition, ventilation was stopped for breath-hold simulation. Data were acquired from a test bolus (20 ml) to determine the timing of peak contrast. For CTA (retrospective ECG gating, slice thickness 0.65 mm, gantry rotation time 350 ms, 120 kV, 600 mAs), 16 ml contrast agent (Iodixanol 320 g/ml, Visipaque; GE Healthcare, Princeton, NJ) was injected at a rate of 4 ml/s, followed by infusion of 40 ml of a 30%/70% contrast/saline mixture at a rate of 4 ml/s, followed by 50 ml saline.

After imaging, the thoracotomy was reopened and the suture was tightened to occlude the vessel. Monastral blue (0.5 ml/kg) was injected into the left atrium to stain the myocardium remote to the stenotic vessel territory. The animal was then killed with saturated potassium chloride solution, and the heart was excised and was put into 10% formaldehyde for 12–18 h.

Ex vivo tissue analysis/microsphere flow

After fixation, the left ventricle (LV) was surgically isolated, excessive fat and connective tissue was removed, and six or seven macroscopic short axis slices of approximately 1 cm thickness were created. Slices were photographed and the area with absence of Monastral blue staining was defined as area at risk by planimetry. Each myocardial slice was divided radially into 16 wedges/sectors. The myocardium from each sector was weighted and microsphere-derived radioactivity was determined in a gamma counter. MBF was then calculated for the segment as previously described [25]. From 16 wedges per slice, adjacent wedges were paired to form eight segments per short axis slice. Values of neighbouring short-axis slices were then averaged to form three ventricular rings and an apical segment. These three rings with eight segments each, together with the apical segment formed a total of 25 segments for the LV, similar to the segmental division used subsequently for PET analysis.

PET and CTA analysis

Multiphase thin slice volumetric CTA data were analysed using multiplane maximum intensity projections by two independent observers blinded to the surgical procedure.

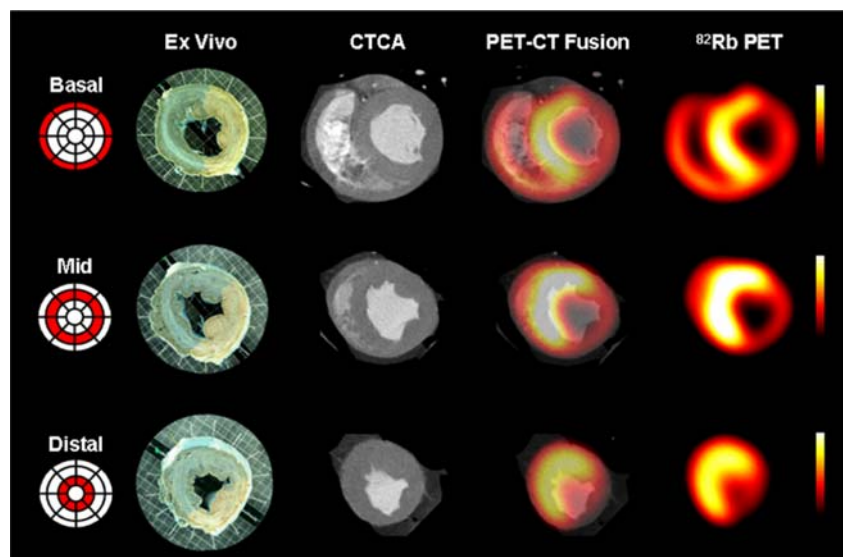
The stenotic vessel was identified and, based on CT morphology, coronary artery vascular territories were assigned to myocardial segments for each dog in order to match CT, PET and ex vivo data based on individual morphology (Fig. 1).

List-mode 2-D PET data were resampled to attenuation corrected, iteratively reconstructed, static (90 s prescan delay), ECG-gated (eight bins for the cardiac cycle), and dynamic images (32 frames for 8 min; 20×6 s, 5×12 s, 4×30 s, 3×60 s). Since misalignment of CT and PET affects the tracer uptake, alignment for attenuation correction was checked using fusion software in all studies, and was excellent in all cases (due to lack of motion in the anaesthetized animals); thus no realignment was necessary [23]. Then, using previously validated software [26], PET data were volumetrically sampled and polar maps of left ventricular myocardial activity were generated. These were used for further analysis.

For comparison to microspheres, maps were divided into the apex and three ventricular rings with eight radial segments, yielding a total of 25 segments. Static rubidium images were integrated with CTA, and stenotic segments were defined as those which were located distal to the stenosis in the vascular territory of the respective vessel, and which were not dyed with Monastral blue ex vivo. Nonstenotic segments were identified as not supplied by the stenotic vessel and the presence of dye ex vivo. LV defect size was measured with the threshold of 60% of the individual LV maximum in order to simulate clinical conditions.

The ejection fraction was measured from gated CT and PET images in six dogs. Automatic wall contour detection was used and individually modified to obtain proper systolic and diastolic LV measurements. Regional wall

Fig. 1 Short axis slices of a representative dog heart. Ex vivo Monastral blue dyed slices were matched with in vivo CT coronary angiography (CTCA) and PET data. All available slices were merged to correlate flow in a 25-segment model, as shown in the polar map schemes on the left



motion was assessed in five myocardial regions (anterior, lateral, septal, inferior and apex) and graded on a four-point scale (0 normal, 1 hypokinesia, 2 akinesia, 3 dyskinesia) in a blinded fashion.

Noninvasive quantification of MBF

Segments defined for static polar maps were reapplied to dynamic imaging series in order to obtain myocardial time–activity curves. Additionally, a small region of interest was positioned in the LV cavity to obtain the arterial input function. Utilizing these data, MBF was quantitatively analysed by two different methods (Fig. 2). First, the first 120 s of the curves was fitted to a standard two-compartment model to obtain rate constants K_1 and k_2 for exchange between blood and tissue [19]. The model fits the real arterial input function and tissue curves, without additional tissue modelling, and it includes a spill-over term to correct for partial volume effects (Rb2C). A previously established formula was employed to extrapolate from the derived K_1 to MBF by considering the nonlinear relationship between tracer extraction and flow [9, 19]. Then, a simplified retention approach (RbRET) was employed by normalizing myocardial activity concentration between minutes 4 and 8 (based on the assumption that myocardial

retention is stable during this interval) to the area under the arterial input function in the first 120 s [9, 10, 19]. The resulting retention index was corrected using fixed terms for partial volume, spill-over and nonlinear extraction as previously described [19].

Quantification with both methods was performed using the custom software MunichHeart, which has been previously validated for other quantitative PET analyses [26]. The analysis requires transfer of dynamic data to a dedicated work-station running the software (2–3 min), and the entire process of reangulating the transaxial images, creating a polar map of myocardial segments, creating time–activity curves for all myocardial segments, creating additional time–activity curves from the LV cavity, fitting the curves to the respective flow model, performing quality control of the fits, and creating a final parametric polar map of MBF takes no more than 10–15 min and can be done by physicians or experienced technologists. This suggests that the procedure is technically feasible in the clinical setting.

In order to describe the relationship between rubidium extraction and flow, noncorrected K_1 from Rb2C was plotted against microsphere MBF and a weighted fit was performed using a generalized Renkin-Crone function (Fig. 3). The relationship was well described by the equation $K_1 = (1 - 0.89 \times e^{-0.68/\text{MBF}}) \times \text{MBF}$, which closely

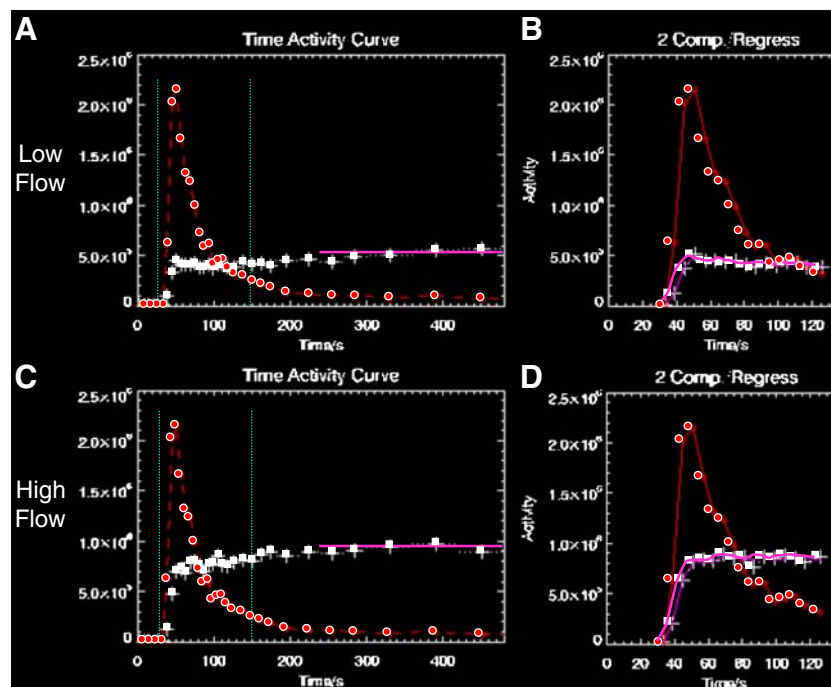


Fig. 2 Quantitative analysis of dynamic ^{82}Rb datasets. Representative time–activity curves for arterial blood (red) and myocardial segments (white), for low-flow regions (a, b) and high-flow regions (c, d) in the same animal. The whole 8-min acquisition is used for calculation of a retention index (a, c). The average activity concentration at 4–8 min

(purple line) is normalized to the area under the arterial blood curve in the first 2 min after injection (green vertical lines indicate margins). For two-compartment model fitting, the first 2 min of the datasets are used (b, c). The fitted tissue curve is indicated in purple

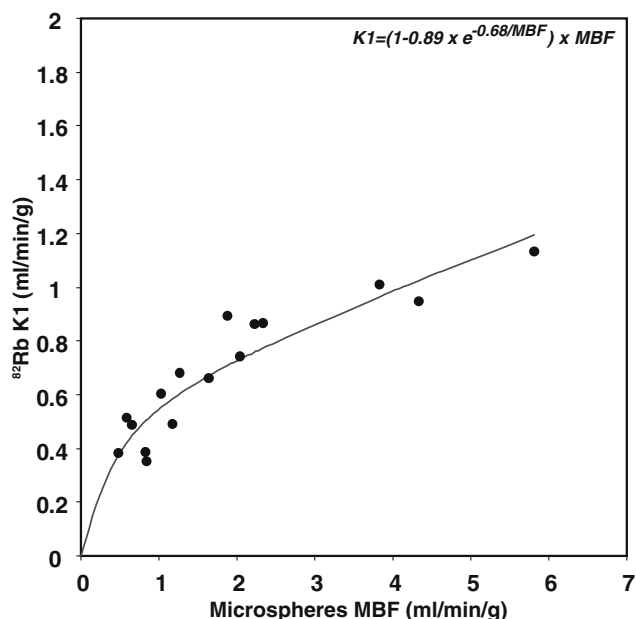


Fig. 3 Relationship between noncorrected K1 for ^{82}Rb from two-compartment modelling and microsphere-derived MBF fitted to a Renkin-Crone function and indicating significant underestimation of flow by K1 due to nonlinear roll-off of the extraction fraction at higher flow

resembles the previously published equation $K1 = (1 - 0.85 \times e^{-0.45/MBF}) \times MBF$ [9, 19], and confirms underestimation of MBF by K1. To obtain the MBF values in the current study, we decided to stay with the previously published formula to avoid a systematic bias.

Reproducibility of flow quantification

Interobserver agreement of both methods for flow analysis was tested by two experienced physicians who were blinded to the results of the other observer and microsphere measurements. For assessment of intraobserver reproducibility, one observer repeated the analysis 3 months after the initial analysis. The analysis process tested for reproducibility included all steps of flow quantification, from reangulation of the transaxial data to generation of parametric polar maps. Results for stenotic and nonstenotic regions were compared.

Statistical analysis

Data are presented as means \pm SD. SAS 8.2 (Cary, NC) or Med-Calc statistical software package v 9.3.0.0 (Maria-kerke, Belgium) was used for analysis. The nonparametric Wilcoxon rank sum test was used to assess differences between continuous variables. Pearson's correlation coefficients were calculated with Fisher's r-to-z conversion to determine significance, and Bland-Altman analysis was employed to define the relationship between PET and

microsphere flow parameters. Passing-Bablok regression analysis and cumulative sum were used for measuring deviation from linearity. For characterization of inter- and intraobserver variability, coefficients of variability (standard deviation of the difference between two measurements over the mean of the two measurements, expressed as a percentage) were determined. *P* values <0.05 were considered statistically significance.

Results

Coronary morphology and PET-CT integration

The presence and location of coronary narrowing was successfully identified by CTA in seven of the nine dogs (Fig. 4). All animals had a left dominant circulation with the posterior descending artery emanating from the left circumflex artery.

For CT-based assignment of myocardial segments to vascular territories for PET analysis, there was good agreement between two independent observers (weighted $\kappa=0.66$). This image-driven definition of stenotic and nonstenotic vascular territories was in fair agreement with post-mortem definition by dye staining (weighted $\kappa=0.37$). There are several possible reasons for this fair agreement. Firstly, from in vivo angiography data, it is not easy to assign myocardial segments to the territory of a vessel when they are located in the border zone between two morphologically visualized arteries. From ex vivo data, on the other hand, the technique of slicing of the tissue will influence orientation of the cardiac long and short axes, which may not perfectly match the in vivo data. Correct angulation of ex vivo slices, in vivo PET and in vivo CT images is another issue. Thus, for accurate subsequent PET analysis of myocardial tissue perfusion, only segments with concordant results between in vivo CT and ex vivo dye analysis were chosen. This integration resulted in 8 \pm 3 myocardial segments assigned to the individual stenotic region with 9 \pm 3 segments representing the nonstenotic region in each animal.

Qualitative regional perfusion and LV function

Using a threshold of 60% of the individual LV maximum, the average perfusion defect size in static ^{82}Rb images was 32 \pm 22%. This was comparable to the average defect size measured ex vivo using planimetry of undyed myocardium (34 \pm 9%). Post-stress LVEF was 35 \pm 11% by CT and 26 \pm 11% by PET (*p*=0.16). Mild regional hypokinesia in the stenotic region was identified by both techniques with good segmental agreement (average score of 0.5 \pm 0.7 for CT vs 0.7 \pm 0.8 for PET; weighted $\kappa=0.63$).

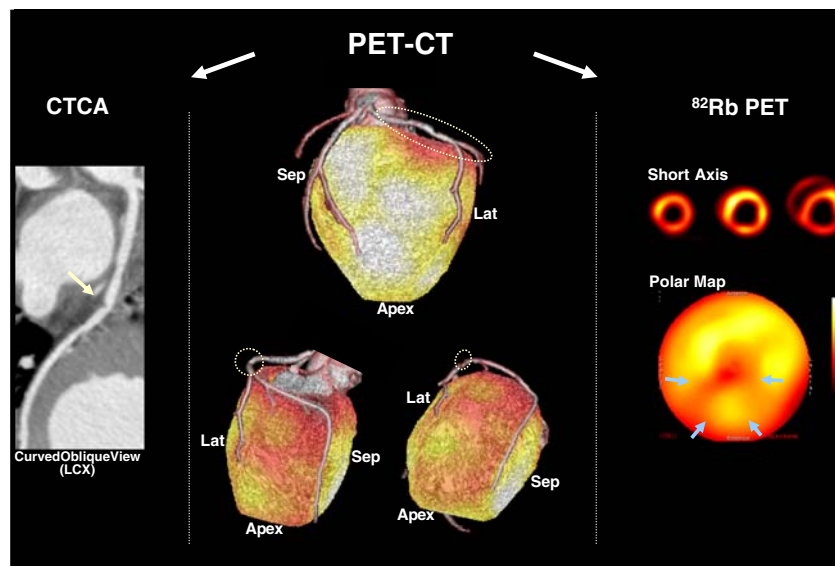


Fig. 4 PET-CT images of a representative dog with experimental coronary stenosis. CT coronary angiography (CTCA, left), shows the arterial narrowing created by a suture in the proximal left anterior descending artery (arrow). PET perfusion imaging with ⁸²Rb (right) shows decreased flow in the entire inferior wall and apex (arrows).

Three-dimensional PET-CT fusion images (centre) show proximal arterial narrowing (circles), a dominant left circumflex artery which supplies the posterior descending artery, and reduced perfusion in the area of this artery

Quantification of myocardial blood flow

Table 1 summarizes average microsphere-derived MBF during adenosine infusion and MBF from ⁸²Rb dynamic analysis after extraction fraction correction according to previously established data [9, 19]. As expected, values were lower in stenotic than in nonstenotic regions, and there was no significant difference between the techniques. Over the entire flow range, MBF from Rb2C was in good agreement with microsphere-derived flow ($y=0.84x + 0.20$; $r=0.92$, $p<0.0001$; Fig. 5a). Bland-Altman analysis showed a mean difference of 0.09 ml/g per minute (95% CI -1.06–1.24; Fig. 5b), and Passing-Bablok regression showed no significant deviation from linearity. MBF by RbRET also correlated significantly with microsphere-derived flow ($y=0.47x + 0.52$; $r=0.75$, $p=0.0004$; Fig. 5c), although the low slope indicates systematic underestimation. Bland-Altman analysis showed a mean difference of 0.45 ml/g per minute

(95% CI -1.51–2.40; Fig. 5d) and Passing-Bablok regression showed no significant deviation from linearity.

When restricting analysis to a more physiological flow range (<3 ml/g per minute), the correlation between RbRET derived MBF and microsphere flow was significantly improved ($y=0.62x + 0.29$; $r=0.84$, $p=0.0001$), and even higher than the two-compartment model approach ($y=0.54x + 0.53$; $r=0.53$, $p=0.042$; Fig. 6). With this flow range, Bland-Altman analysis showed a mean difference of 0.17 ml/g per minute (95% CI -0.51–0.86), and Passing-Bablok regression showed no significant deviation from linearity for RbRET derived MBF and microsphere flow. For the two-compartment model and microsphere flow, a mean difference of 0.04 ml/g per minute (95% CI -1.17–1.25) was observed, and Passing-Bablok regression showed no significant deviation from linearity for Rb2C.

Intraobserver agreement was excellent for both PET flow quantification methods with $r=0.99$ ($p<0.001$) for RbRET

Table 1 MBF measured with Rb and microspheres (n=9). The data presented are means±SD (range)

Method	MBF (ml/g/min)			p value ^a
	Stenotic region	Nonstenotic region	Average in all segments	
Microspheres	1.30±1.22 (0.48–4.33)	2.31±1.60 (0.85–5.81)	1.80±1.48 (0.48–5.81)	0.004
Rb2C	1.34±1.07 (0.44–3.91)	2.08±1.56 (0.58–5.11)	1.71±1.35 (0.44–5.11)	0.027
RbRET	0.98±0.56 (0.51–2.01)	1.73±1.08 (0.70–4.31)	1.36±0.92 (0.51–4.31)	0.027

^a Difference between stenotic and nonstenotic regions.

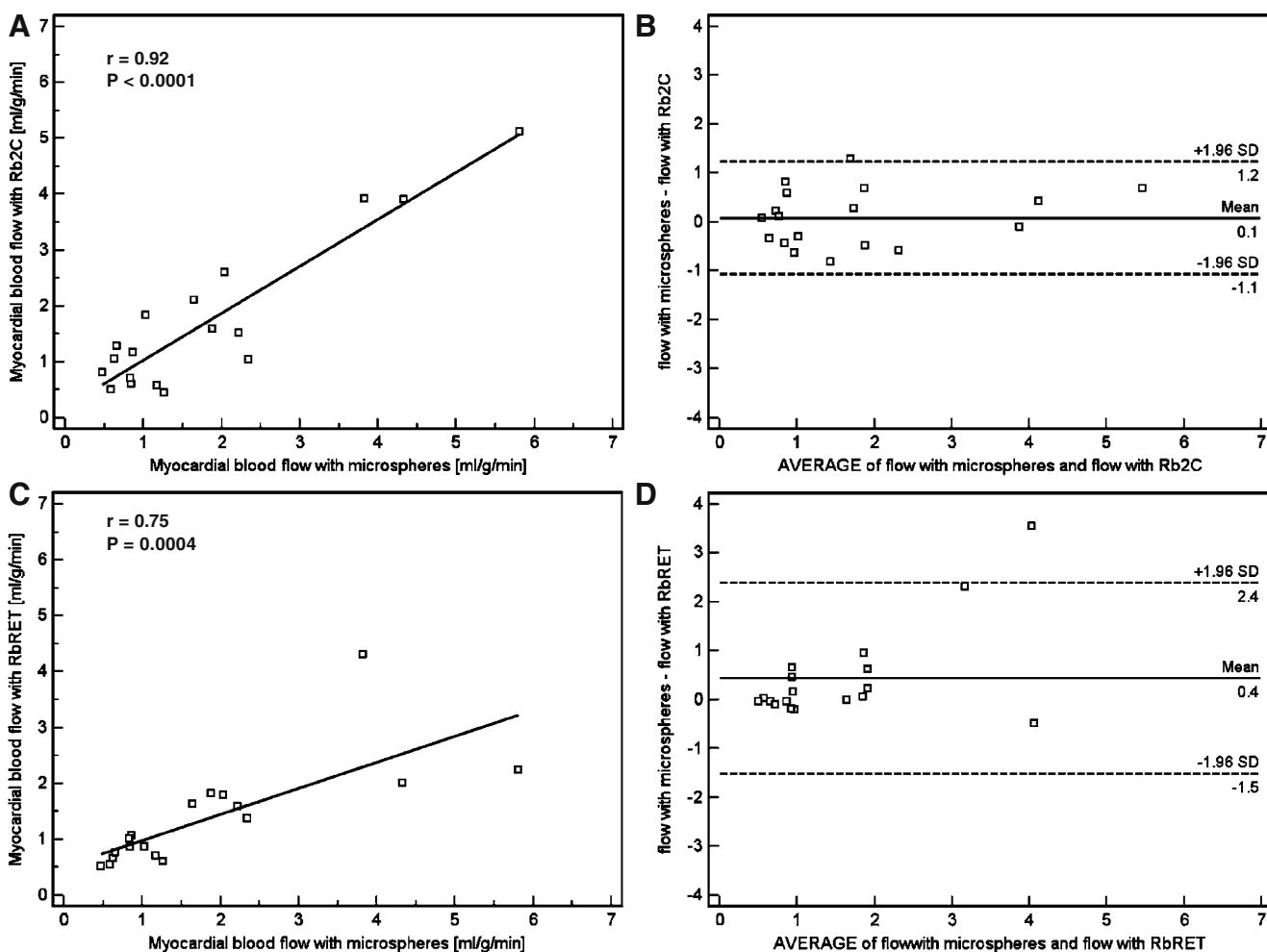


Fig. 5 Regression plots (**a**, **c**), and Bland-Altman plots (**b**, **d**) for microsphere-determined blood flow and dynamic ^{82}Rb PET-CT-derived flow over the entire flow range, using (**a**, **b**) two-compartment

(coefficient of variability $7\pm 9\%$) and $r=0.95$ ($p<0.001$) for Rb2C (coefficient of variability $17\pm 15\%$). In addition, interobserver agreement was excellent for RbRET ($r=0.98$; $p<0.001$; coefficient of variability $8\pm 8\%$) and for Rb2C ($r=0.96$; $p<0.001$; coefficient of variability $14\pm 12\%$).

Discussion

In summary, our data suggest that noninvasive quantification of MBF is feasible using ^{82}Rb and dynamic imaging with latest generation PET-CT systems. Both a standard two-compartment model approach and a simplified retention approach yielded values which correlated well with the gold standard of microsphere-derived flow. Two-compartment modelling was more accurate across the whole range of flow while the retention approach underestimated high flow. The simplified retention approach, however, seemed to be accurate in the lower flow range, which is more

modelling (Rb2C), as well as (**c**, **d**) a retention approach (RbRET) after extraction correction

common in the clinical setting of coronary artery disease. The results of this study should stimulate a broader implementation of quantitative flow measurements into clinical diagnostic algorithms using hybrid imaging methodology.

The widespread availability of ^{82}Rb as a generator product, which can be used at PET sites without a cyclotron, has been a major factor in the success and increasing clinical acceptance of cardiac PET in North America. Its accuracy is superior to that of conventional single photon emission computed tomography (SPECT) [1], the ultrashort tracer half-life allows rapid scanning protocols and high patient throughput [27], and the prognostic value in predicting cardiac events has been demonstrated [6, 28]. Most recently, initial experience with ^{82}Rb has also been reported in European centres [8], and a more widespread availability is to be expected. Despite its increasing success, one of the most powerful features of PET, namely the potential for absolute quantification, is not

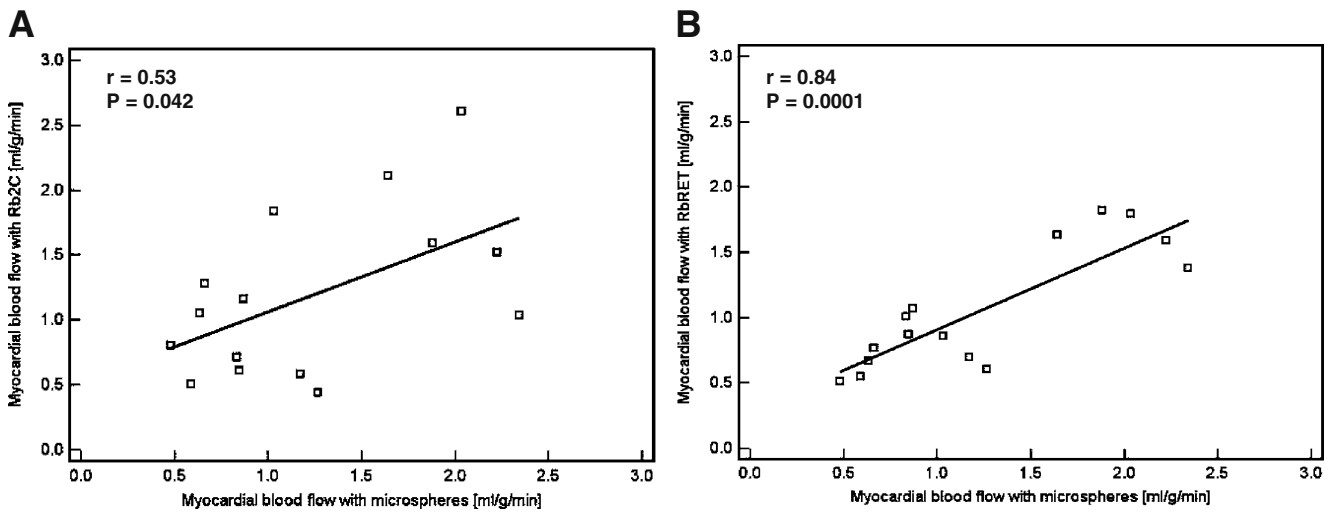


Fig. 6 Regression plots for microsphere-determined blood flow and dynamic ^{82}Rb PET-CT-derived flow in the physiological flow range below 3 ml/g per minute, using (a) two-compartment modelling

(Rb2C), and (b) a retention approach (RbRET) after extraction correction

yet an established part of diagnostic algorithms with ^{82}Rb , and images are mostly analysed visually or semiquantitatively to interpret relative regional perfusion. But absolute quantification of MBF could be of significant value for several purposes. Firstly, a global flow reserve reduction can help in the identification of balanced ischaemia in extensive coronary artery disease—a source of false negative scans when only relative regional perfusion is analysed [14]. Secondly, flow quantification may help in the detection of impaired regional vasoreactivity in areas not showing visually overt reversibility. Thirdly, absolute flow can be impaired in early stages of coronary disease before development of regional heterogeneity, indicating globally impaired vascular reactivity and endothelial dysfunction. Several studies have suggested that such impairments exist in individuals with extensive risk factors [29–35], and that they are indicative of a more rapid progression towards clinically overt disease and cardiac events [15, 17, 36]. Finally, quantitative flow measurements should be able to sensitively identify improvements in myocardial microcirculation in response to therapeutic and preventive measures [37–39].

Although several groups have suggested that quantification of flow from dynamic ^{82}Rb data is feasible [18–21], there are factors which may have limited clinical application in the past. Firstly, handling and processing of multiframe dynamic datasets used to be laborious and could not be combined with electrocardiographically gated acquisition. This has been overcome by more powerful acquisition tools which generate multichannel list-mode data during acquisition. Raw list-mode data can be reformatted after the acquisition to generate dynamic images, gated images or simple static images, as demon-

strated in the present study. The high reproducibility and the short time necessary for conducting a complete analysis support the clinical practicability of our approach. Secondly, the tracer characteristics of ^{82}Rb with a nonlinear extraction at higher flow rates, as confirmed in the present study, remain a limitation and source of errors. Algorithms for correction need to be implemented to overcome this problem, but any correction will amplify noise and thus inaccuracy. In the present study, we used preestablished formulae to correct the influx constant K_1 or the retention index in order to derive flow. This resulted in accurate estimates of microsphere-derived flow in our animal model, but whether the technique is robust in the clinical setting, where the amount of noise is greater, needs to be demonstrated in a next step. It should also be noted that inaccuracies will occur at high flow due to the plateau of extraction confirmed in our study. This may not be a practical problem in coronary artery disease, where peak flow is attenuated, but it still represents a considerable limitation of ^{82}Rb over other flow tracers such as ^{15}O -water or ^{13}N -ammonia. Finally, the physical characteristics of ^{82}Rb with a very short half-life of 78 s represent a challenge for dynamic analysis of tracer kinetics, because the high amount of injected radioactivity necessary to obtain good-quality static images later after injection can result in scanner dead-time problems and thus inaccuracy in measurements of arterial blood curves due to very high count rates during the first pass of the bolus through the heart. The scanner system used in our study incorporated a new generation of detector material which has lower dead-time and is more sensitive during the high count rate conditions [22]. The resulting improvement is expected to be another advantage for analysis of tracer kinetics from ^{82}Rb .

We tested two approaches for quantification which have been previously introduced: a compartmental model approach and a simplified approach based on retention kinetics. Both approaches yielded values which were in agreement with the gold standard of microsphere-derived flow. Over the entire flow range covered in our study (up to 6 ml/g per minute), the compartment model yielded better correlation and less deviation than the retention approach, which tended to underestimate true flow. With the retention approach, flow is estimated from the average activity concentration during the final 4 minutes of the scan, and the post-hoc correction factor accounts not only for extraction but also for partial volume and spill-over [19]. In contrast, the two-compartment model estimates parameters from kinetic data, which includes a washout constant that cannot be considered in the retention approach, and regional spill-over correction factors that are estimated along with the other parameters. Because the correction factors are smaller, any error in parameter estimates is less amplified, which probably explains the better accuracy in the high flow range. In contrast, when we restricted correlation analysis to the physiological flow range <3 ml/g per minute, which covers most of the values observed in the clinical setting, the retention approach yielded a better agreement with microsphere flow. This is most likely explained by the intrinsic noise and variability of dynamic ^{82}Rb images, which translate into noise of time–activity curves and thus inaccuracies of curve fitting especially when flow, and thus the amount of delivered radiotracer and resultant imaging signal, are low. The retention approach is more robust in this regard because only an activity concentration determined from a longer time interval and an integral under the arterial blood curve go into the equation. Our data thus suggest that the retention approach is a preferable method for clinical quantification of flow in humans, where very high flow is unlikely and data noise is expected to be larger than in our animal model.

While algorithms for absolute flow quantification from ^{82}Rb have been introduced and validated by other groups [10, 18, 19, 21], the present study is the first to use a state-of-the-art hybrid PET-CT system. We made full use of the imaging capabilities of this system by obtaining coronary morphology via CT angiography, which helped us identify experimental stenosis and myocardial segments supplied by the stenotic vessel and by nonstenotic vessels for perfusion analysis. Additionally, both techniques were used for analysis of regional and global function and geometry. It is expected that hybrid PET-CT systems will provide an integrated view of cardiac and coronary anatomy along with tissue function and perfusion. Our study suggests that quantitative flow is another image-derived parameter which can be routinely obtained in order to further increase the strength of the imaging technique.

Some possible limitations need to be considered for translation of our results to the clinical setting. Firstly, in the current study, we used two different doses of adenosine to cause hyperaemia. After six animals, we observed a very narrow range of flow with the clinical dose of adenosine (140 $\mu\text{g}/\text{kg}$ per minute) and therefore tripled the dose for the remaining animals. With the higher dose, we also observed higher flow values. The limited hyperaemia with the lower dose was probably caused by the highly stressful conditions due to open heart surgery directly preceding imaging as well as lengthy cardiodepressive anaesthesia. We compared the PET-derived flow with the gold standard microsphere-derived flow, and thus the method comparison itself was not influenced. However, it should be noted that a tripling of the dose does not reflect common clinical practice. Secondly, our data confirm that ^{82}Rb uptake is nonlinearly related to flow and plateaus at higher flow rates. How much this influences the clinical practicability of flow quantification from ^{82}Rb will need to be determined in various clinical settings. Our study provides the basic science groundwork for future projects. Further, although not the major purpose of our study, we also compared measures of LV function between PET and CT. The results were in good agreement, but both techniques may not necessarily be used interchangeably. Clinical studies have been conducted which provide more valid results for functional data analysed with PET compared to MRI and CT [40, 41]. And finally, it should be noted that our results were obtained using LYSO crystals that are not yet broadly employed, and using 2-D imaging, which is no longer available with cameras of several manufacturers which provide 3-D imaging only. Whether our algorithms are reliable using other crystals or 3-D acquisition will need to be determined in the future.

In conclusion, our results suggest that quantification of MBF is feasible using dynamic PET-CT imaging with ^{82}Rb . A simplified approach based on tracer retention appears most practicable in the physiological flow range. Our study encourages further testing of the robustness and usefulness in the clinical context of cardiac hybrid imaging.

Acknowledgements The authors would like to thank Dr. Martin Lodge for his excellent technical assistance. The study was supported by Donald W. Reynolds Foundation. Dr. Lautamäki is supported by grants from The Finnish Cardiac Research Foundation, The Finnish Medical Foundation, The Instrumentarium Foundation for Science, and by the Bracco/SNM Research Fellowship in Cardiovascular Molecular Imaging.

References

1. Bateman TM, Heller GV, McGhie AI, Friedman JD, Case JA, Bryngelson JR, et al. Diagnostic accuracy of rest/stress ECG-

- gated Rb-82 myocardial perfusion PET: comparison with ECG-gated Tc-99m sestamibi SPECT. *J Nucl Cardiol* 2006;13:24–33.
2. Machac J, Bacharach SL, Bateman TM, Bax JJ, Beanlands R, Bengel F, et al. Positron emission tomography myocardial perfusion and glucose metabolism imaging. *J Nucl Cardiol* 2006;13:e121–e151.
 3. Gould KL, Pan T, Loghin C, Johnson NP, Guha A, Sdringola S. Frequent diagnostic errors in cardiac PET/CT due to misregistration of CT attenuation and emission PET images: a definitive analysis of causes, consequences, and corrections. *J Nucl Med* 2007;48:1112–1121.
 4. Santana CA, Folks RD, Garcia EV, Verdes L, Sanyal R, Hainer J, et al. Quantitative (82)Rb PET/CT: development and validation of myocardial perfusion database. *J Nucl Med* 2007;48:1122–1128.
 5. Sampson UK, Dorbala S, Limaye A, Kwong R, Di Carli MF. Diagnostic accuracy of rubidium-82 myocardial perfusion imaging with hybrid positron emission tomography/computed tomography in the detection of coronary artery disease. *J Am Coll Cardiol* 2007;49:1052–1058.
 6. Yoshinaga K, Chow BJ, Williams K, Chen L, deKemp RA, Garrard L, et al. What is the prognostic value of myocardial perfusion imaging using rubidium-82 positron emission tomography. *J Am Coll Cardiol* 2006;48:1029–1039.
 7. Kaufmann PA. 82-Rubidium – the dawn of cardiac PET in Europe. *Eur J Nucl Med Mol Imaging* 2007;34:1963–1964.
 8. Groves AM, Speechly-Dick ME, Dickson JC, Kayani I, Endozo R, Blanchard P, et al. Cardiac (82)rubidium PET/CT: initial European experience. *Eur J Nucl Med Mol Imaging* 2007;34:1965–1972.
 9. Mullani NA, Goldstein RA, Gould KL, Marani SK, Fisher DJ, O'Brien HA Jr, et al. Myocardial perfusion with rubidium-82. I. Measurement of extraction fraction and flow with external detectors. *J Nucl Med* 1983;24:898–906.
 10. Mullani NA, Gould KL. First-pass measurements of regional blood flow with external detectors. *J Nucl Med* 1983;24:577–581.
 11. Huang SC, Williams BA, Krivokapich J, Araujo L, Phelps ME, Schelbert HR. Rabbit myocardial 82Rb kinetics and a compartmental model for blood flow estimation. *Am J Physiol* 1989;256:H1156–H1164.
 12. Herrero P, Markham J, Shelton ME, Weinheimer CJ, Bergmann SR. Noninvasive quantification of regional myocardial perfusion with rubidium-82 and positron emission tomography. Exploration of a mathematical model. *Circulation* 1990;82:1377–1386.
 13. Stewart RE, Schwaiger M, Molina E, Popma J, Gacioch GM, Kalus M, et al. Comparison of rubidium-82 positron emission tomography and thallium-201 SPECT imaging for detection of coronary artery disease. *Am J Cardiol* 1991;67:1303–1310.
 14. Parkash R, deKemp RA, Ruddy TD, Kitsikis A, Hart R, Beauchesne L, et al. Potential utility of rubidium 82 PET quantification in patients with 3-vessel coronary artery disease. *J Nucl Cardiol* 2004;11:440–449.
 15. Schindler TH, Nitzsche EU, Schelbert HR, Olschewski M, Sayre J, Mix M, et al. Positron emission tomography-measured abnormal responses of myocardial blood flow to sympathetic stimulation are associated with the risk of developing cardiovascular events. *J Am Coll Cardiol* 2005;45:1505–1512.
 16. Schindler TH, Nitzsche E, Magosaki N, Brink I, Mix M, Olschewski M, et al. Regional myocardial perfusion defects during exercise, as assessed by three dimensional integration of morphology and function, in relation to abnormal endothelium dependent vasoreactivity of the coronary microcirculation. *Heart* 2003;89:517–526.
 17. Schachinger V, Britten MB, Zeiher AM. Prognostic impact of coronary vasodilator dysfunction on adverse long-term outcome of coronary heart disease. *Circulation* 2000;101:1899–1906.
 18. Herrero P, Markham J, Shelton ME, Bergmann SR. Implementation and evaluation of a two-compartment model for quantification of myocardial perfusion with rubidium-82 and positron emission tomography. *Circ Res* 1992;70:496–507.
 19. Yoshida K, Mullani N, Gould KL. Coronary flow and flow reserve by PET simplified for clinical applications using rubidium-82 or nitrogen-13-ammonia. *J Nucl Med* 1996;37:1701–1712.
 20. El Fakhri G, Sitek A, Guerin B, Kijewski MF, Di Carli MF, Moore SC. Quantitative dynamic cardiac 82Rb PET using generalized factor and compartment analyses. *J Nucl Med* 2005;46:1264–1271.
 21. Lortie M, Beanlands RS, Yoshinaga K, Klein R, Dasilva JN, deKemp RA. Quantification of myocardial blood flow with 82Rb dynamic PET imaging. *Eur J Nucl Med Mol Imaging* 2007;34:1765–1774.
 22. Kemp BJ, Kim C, Williams JJ, Ganin A, Lowe VJ. NEMA NU 2–2001 performance measurements of an LYSO-based PET/CT system in 2D and 3D acquisition modes. *J Nucl Med* 2006;47:1960–1967.
 23. Lautamaki R, Brown TL, Merrill J, Bengel FM. CT-based attenuation correction in (82)Rb-myocardial perfusion PET-CT: incidence of misalignment and effect on regional tracer distribution. *Eur J Nucl Med Mol Imaging* 2008;35:305–310.
 24. Schwaiger M, Ziegler S, Nekolla SG. PET/CT: challenge for nuclear cardiology. *J Nucl Med* 2005;46:1664–1678.
 25. Glover DK, Ruiz M, Edwards NC, Cunningham M, Simanis JP, Smith WH, et al. Comparison between 201Tl and 99mTc sestamibi uptake during adenosine-induced vasodilation as a function of coronary stenosis severity. *Circulation* 1995;91:813–820.
 26. Nekolla SG, Miethaner C, Nguyen N, Ziegler SI, Schwaiger M. Reproducibility of polar map generation and assessment of defect severity and extent assessment in myocardial perfusion imaging using positron emission tomography. *Eur J Nucl Med* 1998;25:1313–1321.
 27. Machac J. Cardiac positron emission tomography imaging. *Semin Nucl Med* 2005;35:17–36.
 28. Marwick TH, Shan K, Patel S, Go RT, Lauer MS. Incremental value of rubidium-82 positron emission tomography for prognostic assessment of known or suspected coronary artery disease. *Am J Cardiol* 1997;80:865–870.
 29. Di Carli MF, Bianco-Battles D, Landa ME, Kazmers A, Groehn H, Muzik O, et al. Effects of autonomic neuropathy on coronary blood flow in patients with diabetes mellitus. *Circulation* 1999;100:813–819.
 30. Laine H, Raitakari OT, Niinikoski H, Pitkanen OP, Iida H, Viikari J, et al. Early impairment of coronary flow reserve in young men with borderline hypertension. *J Am Coll Cardiol* 1998;32:147–153.
 31. Sundell J, Laine H, Luotolahti M, Kalliokoski K, Raitakari O, Nuutila P, et al. Obesity affects myocardial vasoreactivity and coronary flow response to insulin. *Obes Res* 2002;10:617–624.
 32. Pitkanen OP, Nuutila P, Raitakari OT, Porkka K, Iida H, Nuotio I, et al. Coronary flow reserve in young men with familial combined hyperlipidemia. *Circulation* 1999;99:1678–1684.
 33. Pitkanen OP, Raitakari OT, Niinikoski H, Nuutila P, Iida H, Voipio-Pulkki LM, et al. Coronary flow reserve is impaired in young men with familial hypercholesterolemia. *J Am Coll Cardiol* 1996;28:1705–1711.
 34. Momose M, Abletshauer C, Neverve J, Nekolla SG, Schnell O, Standl E, et al. Dysregulation of coronary microvascular reactivity in asymptomatic patients with type 2 diabetes mellitus. *Eur J Nucl Med Mol Imaging* 2002;29:1675–1679.
 35. Dorbala S, Hassan A, Heinonen T, Schelbert HR, Di Carli MF. Coronary vasodilator reserve and Framingham risk scores in subjects at risk for coronary artery disease. *J Nucl Cardiol* 2006;13:761–767.
 36. Halcox JP, Schenke WH, Zalos G, Mincemoyer R, Prasad A, Waclawiw MA, et al. Prognostic value of coronary vascular endothelial dysfunction. *Circulation* 2002;106:653–658.

37. Higuchi T, Abletshauer C, Nekolla SG, Schwaiger M, Bengel FM. Effect of the angiotensin receptor blocker Valsartan on coronary microvascular flow reserve in moderately hypertensive patients with stable coronary artery disease. *Microcirculation* 2007;14:805–812.
38. Lautamaki R, Airaksinen KE, Seppanen M, Toikka J, Harkonen R, Luotolahti M, et al. Insulin improves myocardial blood flow in patients with type 2 diabetes and coronary artery disease. *Diabetes* 2006;55:511–516.
39. Guethlin M, Kasel AM, Coppenrath K, Ziegler S, Delius W, Schwaiger M. Delayed response of myocardial flow reserve to lipid-lowering therapy with fluvastatin. *Circulation* 1999;99:475–481.
40. Slart RH, Bax JJ, de Jong RM, de Boer J, Lamb HJ, Mook PH, et al. Comparison of gated PET with MRI for evaluation of left ventricular function in patients with coronary artery disease. *J Nucl Med* 2004;45:176–182.
41. Chander A, Brenner M, Lautamaki R, Voicu C, Merrill J, Bengel FM. Comparison of measures of left ventricular function from electrocardiographically gated ^{82}Rb PET with contrast-enhanced CT ventriculography: a hybrid PET-CT analysis. *J Nucl Med* 2008;49:1643–1650.